



Cite this: *Soft Matter*, 2019, 15, 6830

Disordered hyperuniform obstacles enhance sorting of dynamically chiral microswimmers†

Jie Su,  Huijun Jiang * and Zhonghuai Hou *

Disordered hyperuniformity, a brand new type of arrangement with novel physical properties, provides various practical applications in extensive fields. To highlight the great potential of applying disordered hyperuniformity to active systems, a practical example is reported here by an optimal sorting of dynamically chiral microswimmers in disordered hyperuniform obstacle environments in comparison with regular or disordered ones. This optimal chirality sorting stems from a competition between advantageous microswimmer–obstacle collisions and disadvantageous trapping of microswimmers by obstacles. Based on this mechanism, optimal chirality sorting is also realized by tuning other parameters including the number density of obstacles, the strength of driven force and the noise intensity. Our findings may open a new perspective on both theoretical and experimental investigations for further applications of disordered hyperuniformity in active systems.

Received 30th May 2019,
Accepted 29th July 2019

DOI: 10.1039/c9sm01090d

rsc.li/soft-matter-journal

1 Introduction

The hyperuniform point pattern possesses the property that the variance of the point number contained within a regularly shaped observation window grows more slowly than its volume,^{1,2} differing from disordered patterns. Equivalently, a hyperuniform point pattern possesses a structure factor dependent on the small-wavenumber in a power-law form, *i.e.*, $S(\mathbf{k}) \sim |\mathbf{k}|^\alpha$ for $|\mathbf{k}| \rightarrow 0$. Disordered hyperuniform (DH) patterns are states lying between crystals (regular patterns) and liquids (disordered patterns), which suppress large-scale density fluctuations like crystals, and lack any conventional long-range order like liquids or glasses.³ The positive exponent α represents a rough distinction between regular and DH patterns, *i.e.*, the point pattern is DH for limited α , but becomes stealthy,^{4–6} even becoming a regular point pattern⁷ when $\alpha \rightarrow \infty$. In recent decades, DH structures have been widely discovered in many natural systems, including matter distribution in the Universe,^{8,9} avian cone photoreceptors,^{10,11} the ground state of liquid ⁴He,^{12–14} and some aperiodic tilings,^{1,8,15,16} to list just a few. Besides, DH materials can also be conveniently synthesized in experiments by self-assembling of block-copolymer micelles,¹⁷ and periodically driven emulsions,¹⁸ and many other methods.^{19,20} The distinct structure of DH patterns then provides various potential applications in extensive fields, such as surface-enhanced Raman spectroscopy,^{21,22} various photonic applications at the micro- and nanoscales,^{23–25} THz quantum cascade lasers,²⁶ diffusion and conduction transport through DH media,^{27,28} *etc.*

As one of the hottest research topics in recent years across physical, chemical, materials and biological sciences, active systems have the ability to take in and dissipate energy from the environment so as to drive themselves far from equilibrium.²⁹ Active systems exhibit novel behaviors in comparison with their passive counterparts, such as emergence of dynamic chirality,^{30–35} activity-induced phase separation,^{36,37} collective vortex,^{38,39} polar swarms,⁴⁰ *etc.*^{41–45} It is also reported that active particles show rather different behaviors in complex environments in comparison to passive ones.^{46–49} It is then a great opportunity to introduce the concept of disordered hyperuniformity to active systems, where new exciting behaviors may emerge.

In this paper, we report a practical example to highlight the potential of applying DH structures to active systems by a DH-pattern-enhanced sorting of dynamically chiral microswimmers (DCMSs). DCMSs taking a circular motion^{30–34} provide a routine for sorting of the microswimmers themselves or other particles coupled to them when they are driven through an obstacle environment,^{50–53} even in the situation where particle separation can be hardly achieved by mechanical means.⁵⁴ Here, the sorting efficiencies are compared through a series of two-dimensional obstacle environments designed with patterns of regular, DH, or disordered types. Remarkably, an optimal sorting of DCMSs is observed in DH obstacles. Detailed analysis reveals that, as the pattern changes from regular to DH and then to disordered, on the one hand, the collision probability between DCMSs and obstacles increases, facilitating sorting of DCMSs, and on the other hand, more and more DCMSs are found to be trapped by the obstacles, which hinders the efficiency of the chirality separation. The observed optimal chirality sorting in DH obstacles is then a consequence of the competition between these two effects. Based on this mechanism, the influences of

Department of Chemical Physics & Hefei National Laboratory for Physical Sciences at Microscales, iChEM, University of Science and Technology of China, Hefei, Anhui 230026, China. E-mail: hjjiang3@ustc.edu.cn, hzhlj@ustc.edu.cn

† Electronic supplementary information (ESI) available. See DOI: 10.1039/c9sm01090d

the number density of obstacles and the strength of driven force are also investigated by further intensive simulations. Furthermore, it is found that there is also an optimal chirality sorting induced by noise, *i.e.*, before the noise intensity increases to be large enough to dominate the dynamics and break the chirality sorting, noise can not only amplify the collision probability between microswimmers and obstacles, but also help those captured swimmers jump out of obstacle traps.

2 Model

The detailed setup of the system is shown in Fig. 1(a). A mixture of counterclockwise (CCW) and clockwise (CW) microswimmers are driven through an obstacle environment by a static force $\mathbf{f}_d = f_d \mathbf{e}_x$ parallel to the X -axis, where the force may be realized by an external electric or magnetic field. The CCW and CW swimmers have the same radius R_p and self-propelled rate v_0 except that the angular speed is ω for CCW swimmers and $-\omega$ for CW ones as shown in the top inset. The motion of each DCMS is described by the following overdamped Langevin equations

$$\frac{d\mathbf{r}_i}{dt} = v_0 \mathbf{n}_i + \frac{1}{\gamma} \left[\mathbf{f}_d + \sum_{j \neq i} \mathbf{F}_{ij}^p(\mathbf{r}_{ij}) + \sum_m \mathbf{F}_{im}^o(\mathbf{r}_{im}) \right] + \xi_i. \quad (1)$$

$$\frac{d\phi_i}{dt} = \omega_i + \zeta_i. \quad (2)$$

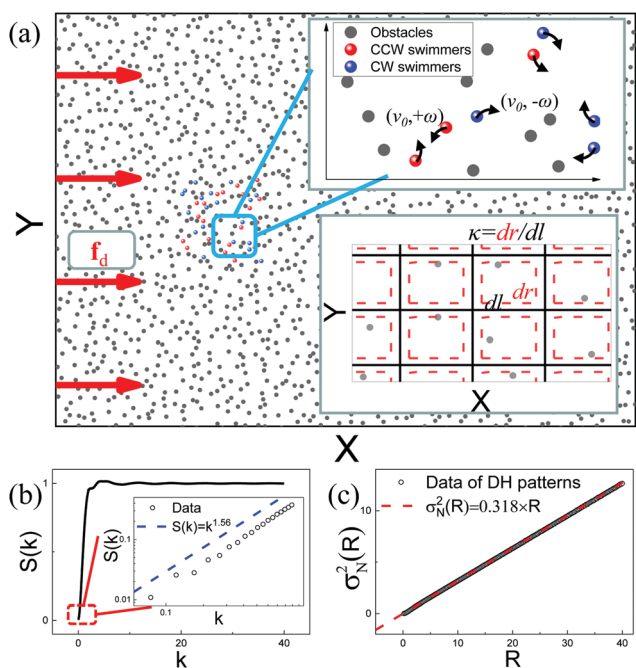


Fig. 1 Schematic of the system. (a) DCMSs (colored spheres) are driven through obstacle environments (gray points) by a static force (red arrows). The top inset is the zoom-in of the blue box with counterclockwise (CCW, red spheres) and clockwise (CW, blue spheres) microswimmers. The bottom inset shows the method to generate different patterns. (b) The structure factor $S(k)$ as a function of the wavenumber k for generated DH obstacles. The inset is the zoom-in near $k \rightarrow 0$. (c) The variance of point number $\sigma_N^2(R)$ as a function of the large window radius R .

Herein, γ is the friction coefficient, $\mathbf{r}_{ij(im)} = \mathbf{r}_i - \mathbf{r}_{j(im)}$, and $\mathbf{n}_i = (\cos(\phi_i), \sin(\phi_i))$ is the propulsion direction of swimmer i with ϕ_i the angle of \mathbf{n}_i . The interaction between DCMSs and that between DCMSs and obstacles are both of the linear spring form with the stiffness constants k_p and k_o ,^{52,53} respectively; hence, the force between the i th and j th swimmers is given by $\mathbf{F}_{ij}^p(\mathbf{r}_{ij}) = k_p(2R_p - r_{ij})\Theta(2R_p - r_{ij})\mathbf{e}_{ij}$, and the force between the i th swimmer and the m th obstacle is $\mathbf{F}_{im}^o(\mathbf{r}_{im}) = k_o(R_p + R_o - r_{im})\Theta(R_p + R_o - r_{im})\mathbf{e}_{im}$, with $r_{ij(im)} = |\mathbf{r}_{ij(im)}|$, $\mathbf{e}_{ij(im)} = \mathbf{r}_{ij(im)}/r_{ij(im)}$, R_o the radius of the obstacle, and $\Theta(x)$ the Heaviside step function of x . ξ_i denotes the random force satisfying the fluctuation-dissipation relation $\langle \xi_{\mu i}(t) \xi_{\nu j}(t') \rangle = 2D_t \delta(t - t') \delta_{\mu\nu} \delta_{ij}$, where the subscript $\mu(\nu)$ denotes the component along the $X(Y)$ -axis, and D_t is the translational diffusion coefficient. The last term ζ_i in eqn (2) is the rotational fluctuation satisfying $\langle \zeta_i(t) \zeta_j(t') \rangle = 2D_o \delta(t - t') \delta_{ij}$ with D_o the rotational diffusion coefficient.

To generate a two-dimensional DH array with number density ρ_o , we use a simple method inspired by Gabrielli *et al.*⁸ as follows: (Step 1) cut the total surface into squares with the same size $dl = \rho_o^{-1/2}$; (Step 2) place a point randomly inside each square. An example of a DH pattern consisting of $N_o = 2500$ points generated by this method is plotted by gray points in Fig. 1(a). The structure factor $S(k)$ averaged over 10^6 ensembles is shown in Fig. 1(b). Clearly, it can be found that $\lim_{k \rightarrow 0} S(k) \sim k^\alpha$ with an exponent $\alpha = 1.56 \pm 0.03$ (the inset of Fig. 1(b)), indicating the DH characteristic of the generated pattern. Moreover, as shown in Fig. 1(c), the number variance $\sigma_N^2(R) \equiv \langle N_\Omega^2 \rangle - \langle N_\Omega \rangle^2$ inside a large window Ω with side R depends linearly on R , further demonstrating that the pattern is of DH type. Note that it is also convenient to generate a regular or disordered pattern by rescaling the squares in Step 2, *i.e.*, randomly place a point in a square of size dr (enclosed by red dashed lines in the bottom inset of Fig. 1(a)), which could be larger or smaller than dl . Naturally, the parameter $\kappa = dr/dl$ can be used to characterize the degree of disorder of the patterns. With this construction, the generated pattern is regular for $\kappa = 0$, DH for κ around 1, and disordered for large enough κ .

In simulations, parameters are made dimensionless by using γ , v_0 and ω as the basic units, so that the basic units for time, length and energy are ω^{-1} , $v_0 \omega^{-1}$ and $v_0^2 \omega^{-1} \gamma$. According to the experimental data for DCMSs,^{33,55} we fix $R_p = R_o = 0.5$, $D_t = 5.0 \times 10^{-3}$, and $D_o = 10^{-2}$, if not otherwise stated. Other parameters are $k_p = k_o = 200$, $f_d = 0.2$, $\rho_o = 0.0977$ and time step $dt = 10^{-3}$. For consistence, all of the following results are obtained from a mixture of 2000 CCW and 2000 CW swimmers running for a long time $t_{\text{final}} = 4 \times 10^4$. The initial positions of these DCMSs are randomly chosen in a rectangle (200×100) near the origin.

3 Result

First of all, we are interested in how the degree of disorder of the obstacle affects the collective behaviors of DCMSs. Typical trajectories of individual swimmers as well as the averaged ones over all CCW (or CW) swimmers for $\kappa = 1.0$ are plotted in the left inset of Fig. 2 (also can be seen in Movie S1, ESI†). It can be

observed that all the CCW swimmers move along the negative direction of the Y -axis while all the CW swimmers move along the positive one, resulting in a clear sorting of DCMs.

In order to quantitatively measure the efficiency of chirality sorting, we introduce an order parameter

$$\Delta L_{\text{sep}} = \langle Y_{\text{cw}}(t_{\text{final}}) \rangle - \langle Y_{\text{ccw}}(t_{\text{final}}) \rangle, \quad (3)$$

where $Y_{\text{cw(ccw)}}$ denotes the Y -position of CW(CCW) swimmers, $\langle \cdot \rangle$ means averaging over all CW(CCW) swimmers, such that ΔL_{sep} shows the difference between the centers of these two groups of DCMs in the Y -direction. Dependence of ΔL_{sep} on the degree of disorder κ of the obstacle environment is shown in Fig. 2. It can be seen that ΔL_{sep} increases as κ increases from 0 to 1, and then trails off when κ passes through 1, *i.e.*, obstacle patterns with $\kappa = 1$ most favorably enhance ΔL_{sep} to the largest level. Notice that $\kappa = 1$ corresponds to obstacles with the DH feature mentioned above; the observation thus indicates that the sorting of DCMs in a DH environment is indeed more efficient than the regular or disordered ones.

To check whether a complete sorting of DCMs can be obtained, we introduce another order parameter S to describe the sorting selectivity,

$$S = \int_0^{\infty} P_{\text{cw}}(Y) dY - \int_0^{\infty} P_{\text{ccw}}(Y) dY, \quad (4)$$

where $P_{\text{cw(ccw)}}(Y)$ is the probability distribution of $Y_{\text{cw(ccw)}}$. If all CW swimmers move to $Y > 0$ ($Y < 0$) and all CCW swimmers move to $Y < 0$ ($Y > 0$), *i.e.*, swimmers with different dynamic chirality can be separated completely, one has $S = +1$ ($S = -1$). The obtained S as a function of κ is presented in the right inset of Fig. 2. $S \approx 1$ for $\kappa \leq 1$, and it decreases to be smaller than 1 for $\kappa > 1$, indicating that complete chirality sorting can be achieved for hyperuniform patterns rather than disordered ones. Therefore, the obstacle with the DH feature is the best for the sorting efficiency of DCMs with 100% sorting selectivity.

In order to figure out the underlying mechanism for the DH-pattern-induced optimal sorting of DCMs, we first focus

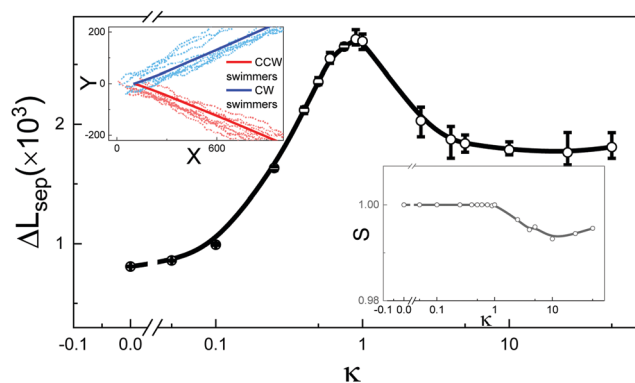


Fig. 2 The difference between the centers of the CW and CCW groups in the Y -direction ΔL_{sep} as a function of the degree of disorder κ . The left inset shows typical individual trajectories (light red and blue dashed lines) and average ones (dark red and blue solid lines) over all CCW (or CW) swimmers for $\kappa = 1.0$ (DH patterns). The right inset shows the dependence of the sorting selectivity S on κ .

on the behaviors during a single collision between DCMs and obstacles. When a DCMs collides with an obstacle, it will rotate the self-propulsion direction in order to move away from the obstacle. Taking a CCW swimmer as an example, as presented in Fig. 3(a), three cases are demonstrated for different collision angle θ between the vector pointing from the CCW swimmer to the obstacle and the X -axis. For $\theta = 0$, the CCW swimmer will wait until its self-propulsion direction points to the positive direction of the Y -axis and then move away from the obstacle. Such a change of self-propulsion direction then leads to a negative shift of the rotating center in the Y -axis after the collision (the red curve for the motion of the swimmer after collision is lower than the black one before collision, as shown in case 1 in Fig. 3(a)). Oppositely, the CCW swimmer would move along the positive Y -direction for $\theta = \pi$ as presented in case 2. Generally, the CCW swimmer colliding with an obstacle at random θ would change its self-propulsion direction to

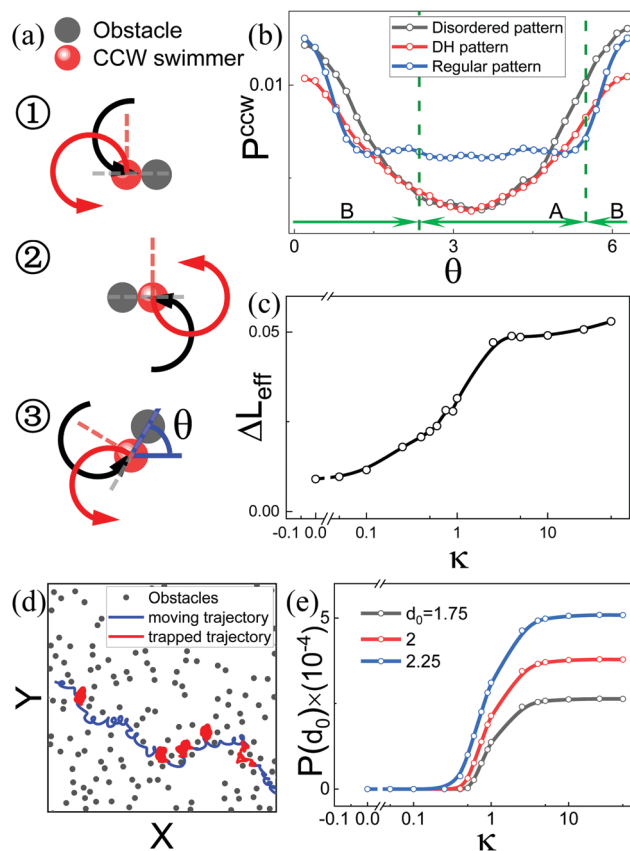


Fig. 3 Underlying mechanism for the optimal sorting of DCMs induced by DH obstacles. (a) Schematic of collisions for $\theta = 0$ (1), π (2) and a general value (3), respectively. The black and red curves represent the motions of the CCW swimmer before and after a collision, respectively. (b) The possibility distribution $P^{\text{CCW}}(\theta)$ of swimmer-obstacle collisions as a function of the collision angle θ for regular, DH or disordered patterns at $f_d = 0.2$. Domains A and B, separated by green dashed lines ($\theta = 3\pi/4$ and $\theta = 7\pi/4$), represent the positive- and negative-shift domains of CCW swimmers. (c) The effective separation length ΔL_{eff} in the Y -direction as a function of κ . (d) A typical trajectory for a CCW swimmer moving (blue segments) or trapped (red segments) in a disordered environment. (e) Possibility $P(d_0)$ of obstacle pairs whose distance is smaller than a given short length d_0 as functions of κ .

$\theta + \pi/2$ in order to move past the obstacle, resulting in a shift $\Delta L_{\text{ccw}} = -v_0\omega^{-1}[\cos(\theta) + \sin(\theta)]$ in the Y -direction after a collision, which is greater than 0 for $\theta \in (3\pi/4, 7\pi/4)$ and less than 0 for $\theta \in [0, 3\pi/4) \cup (7\pi/4, 2\pi)$. A similar mechanism has also been introduced previously in the literature.⁵²

The possibility distribution $P^{\text{ccw}}(\theta)$ of swimmer–obstacle collisions as a function of the collision angle θ for regular, DH or disordered patterns at $f_d = 0.2$ is then shown in Fig. 3(b). Notice that this collision possibility should distribute uniformly in $[0, 2\pi)$ in the case $f_d = 0$, but this uniformity will be broken when a driven force f_d is exerted, so that the collision tends to occur along the direction of the driven force, *i.e.*, P^{ccw} for $\theta \in [0, \pi/2) \cup (3\pi/2, 2\pi)$ (mainly consists of the negative-shift domain in Fig. 3(b)) is larger than that for $\theta \in (\pi/2, 3\pi/2)$ (mainly consists of the positive-shift domain). It is clear that P^{ccw} for the negative-shift domain in Fig. 3(b) is larger than that for the positive-shift one, indicating that CCW swimmers would move along the negative direction of the Y -axis. Moreover, P^{ccw} of the regular pattern is much larger than the other two structures in the positive-shift domain, resulting in the smallest value of averaged ΔL_{ccw} for regular obstacles. Meanwhile, P^{ccw} of the disordered pattern is larger than the DH one in the negative-shift domain, leading to the largest value of averaged ΔL_{ccw} for disordered obstacles. Correspondingly, all the results for CW swimmers are the same except that $\Delta L_{\text{cw}} = v_0\omega^{-1}[\cos(\theta) + \sin(\theta)]$ is larger than 0 for $\theta \in [0, 3\pi/4) \cup (7\pi/4, 2\pi)$ and less than 0 for $\theta \in (3\pi/4, 7\pi/4)$. To quantitatively characterize the effect of collisions, the averaged difference of collision-induced shifts in the Y -direction between CW and CCW swimmers can be measured approximately by $\Delta L_{\text{eff}} = \int_0^{2\pi} (\Delta L_{\text{cw}} P^{\text{cw}} - \Delta L_{\text{ccw}} P^{\text{ccw}}) d\theta$ for a small driven force such as $f_d = 0.2$. As plotted in Fig. 3(c), ΔL_{eff} grows monotonically for increasing κ , indicating that if only independent collisions are taken into account, a larger κ would enhance the sorting efficiency of DCMSSs.

Nevertheless, besides the per-collision effect, obstacles may also trap DCMSSs by multiple collisions if several obstacles are near enough. As an example, as shown in Fig. 3(d), within an obstacle environment with $\kappa = 50$, a CCW swimmer is repeatedly trapped in some neighbouring obstacles for a long time. The trapping effect can be more easily observed for $\kappa = 50$ (disordered patterns, Movie S2, ESI[†]) than $\kappa = 1$ (DH patterns, Movie S1, ESI[†]) or $\kappa = 0$ (regular patterns, Movie S3). In order to depict how the structure of the obstacle environment affects the frequency of traps occurring, we calculate the possibility $P(d_0) = 2N_{d_0}[N_0(N_0 - 1)]$ of obstacle pairs whose distance is smaller than a given short length d_0 for different κ values (Fig. 3(e)). For all chosen d_0 , $P(d_0)$ grows monotonically as κ increases, indicating that as the environment becomes more and more disordered, DCMSSs are more easily trapped, consequently hindering the efficiency of chirality sorting. Therefore, the competition between the advantageous per-collision effect and the disadvantageous multi-collision trapping effect results in an optimal sorting of DCMSSs for κ near 1, *i.e.*, the obstacle with the DH feature.

To fully explore how parameters, including the degree of disorder κ , the number density of obstacles ρ_0 and the driven

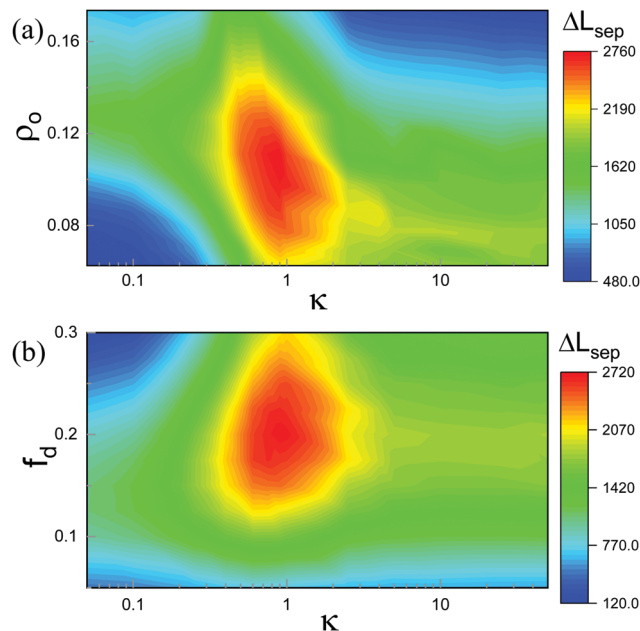


Fig. 4 Sorting of DCMSSs in environments for different obstacle densities and driven forces. The phase diagram for sorting of DCMSSs in the $\kappa - \rho_0$ (a) and $\kappa - f_d$ (b) plane.

force f_d , affect the sorting of DCMSSs, we undertook extensive simulations to obtain the phase diagrams in the $\kappa - \rho_0$ and $\kappa - f_d$ plane (Fig. 4). Interestingly, peaks for ΔL_{sep} are observed in both of these two phase diagrams, indicating that the best sorting efficiency of DCMSSs can be achieved by tuning these three parameters. The optimal chirality sorting for varying ρ_0 or f_d can also be understood based on the aforementioned mechanism as follows. As ρ_0 or f_d increases, although the advantageous per-collision effect between DCMSSs and obstacles increases, the disadvantageous trapping effect of DCMSSs due to multi-collision increases as well. Consequently, the competition of these two opposite effects finally leads to the optimal ΔL_{sep} dependent on ρ_0 or f_d .

Furthermore, according to the above understanding, one can also predict that noise would also be an important factor for sorting of DCMSSs similar to κ . As the noise intensity increases, on the one hand, not only the probability of collisions increases, but also DCMSSs would jump more easily out of obstacle traps, so that a more efficient sorting of DCMSSs can be achieved, and on the other hand, collisions become less and less effective, hindering the chirality separation. Therefore, based on the competition between these two effects, the chirality sorting efficiency should also achieve an optimal value for various noise intensity. This prediction is then verified by further simulations with various noise intensity D_0 and fixed $D_i/D_0 = 0.5$. The obtained dependence of ΔL_{sep} on D_0 for obstacles with disordered ($\kappa = 50$), DH ($\kappa = 1$) and regular ($\kappa = 0$) patterns is plotted in Fig. 5. As expected, an optimal ΔL_{sep} dependence on D_0 can be observed in all of the three patterns, demonstrating the constructive role noise plays in the sorting of DCMSSs through obstacles.

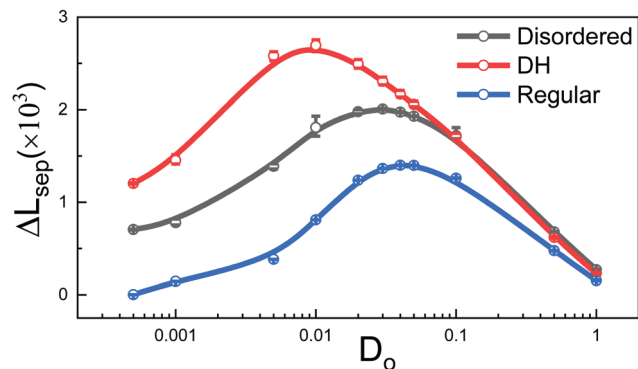


Fig. 5 Dependence of chirality sorting on the noise intensity presented by ΔL_{sep} as functions of D_0 for different patterns.

4 Conclusion

In summary, we found that the sorting of DCMSS driven by a static force performs optimally through an obstacle environment of DH type in comparison with those of regular or disordered ones. This optimal chirality sorting results from the competition between obstacle-induced advantageous collisions and disadvantageous traps of DCMSSs, both of which occur more frequently as the environment changes from regular to DH then disordered patterns. Based on the same competition of the two effects, it was predicted that similar optimal chirality sorting should also be induced by the number density of obstacles, the driven force, or the noise intensity, which was demonstrated by further intensive simulations. The current study provides a convincing example to highlight the great potential of applying disordered hyperuniformity to active systems. Since systems designed with a DH pattern are experimentally available, and active systems are one of the hottest research areas across physical, chemical, materials and biological sciences, our findings may open a new perspective on both theoretical and experimental investigations for further applications of disordered hyperuniformity in active systems in the future.

Conflicts of interest

There are no conflicts to declare.

Acknowledgements

This work is supported by MOST (2016YFA0400904, 2018YFA0208702), NSFC (21833007, 21790350, 21673212, 21521001, 21473165), the Fundamental Research Funds for the Central Universities (2340000074), and Anhui Initiative in Quantum Information Technologies (AHY090200).

References

- 1 S. Torquato and F. H. Stillinger, *Phys. Rev. E: Stat., Nonlinear, Soft Matter Phys.*, 2003, **68**, 041113.
- 2 C. E. Zachary and S. Torquato, *J. Stat. Mech.: Theory Exp.*, 2009, **2009**, P12015.

- 3 S. Torquato, *Phys. Rep.*, 2018, **745**, 1–95.
- 4 S. Torquato, G. Zhang and F. Stillinger, *Phys. Rev. X*, 2015, **5**, 021020.
- 5 Z. Ma and S. Torquato, *J. Appl. Phys.*, 2017, **121**, 244904.
- 6 R. D. Batten, F. H. Stillinger and S. Torquato, *J. Appl. Phys.*, 2008, **104**, 033504.
- 7 E. C. Oğuz, J. E. Socolar, P. J. Steinhardt and S. Torquato, *Phys. Rev. B: Condens. Matter Mater. Phys.*, 2017, **95**, 054119.
- 8 A. Gabrielli, B. Jancovici, M. Joyce, J. Lebowitz, L. Pietronero and F. S. Labini, *Phys. Rev. D: Part. Fields*, 2003, **67**, 043506.
- 9 A. Gabrielli, M. Joyce and F. S. Labini, *Phys. Rev. D: Part. Fields*, 2002, **65**, 083523.
- 10 Y. A. Kram, S. Mantey and J. C. Corbo, *PLoS One*, 2010, **5**, e8992.
- 11 Y. Jiao, T. Lau, H. Hatzikirou, M. Meyer-Hermann, J. C. Corbo and S. Torquato, *Phys. Rev. E: Stat., Nonlinear, Soft Matter Phys.*, 2014, **89**, 022721.
- 12 R. P. Feynman, *Phys. Rev.*, 1954, **94**, 262.
- 13 R. Feynman, *Phys. Rev.*, 1956, **102**, 1189.
- 14 L. Reatto and G. Chester, *Phys. Rev.*, 1967, **155**, 88.
- 15 A. Gabrielli, M. Joyce and S. Torquato, *Phys. Rev. E: Stat., Nonlinear, Soft Matter Phys.*, 2008, **77**, 031125.
- 16 S. H. Hansen, O. Agertz, M. Joyce, J. Stadel, B. Moore and D. Potter, *Astrophys. J.*, 2007, **656**, 631.
- 17 G. Zito, G. Rusciano, G. Pesce, A. Malafronte, R. Di Girolamo, G. Ausanio, A. Vecchione and A. Sasso, *Phys. Rev. E: Stat., Nonlinear, Soft Matter Phys.*, 2015, **92**, 050601.
- 18 J. H. Weijis, R. Jeanneret, R. Dreyfus and D. Bartolo, *Phys. Rev. Lett.*, 2015, **115**, 108301.
- 19 P. M. Piechulla, L. Muehlenbein, R. B. Wehrspohn, S. Nanz, A. Abass, C. Rockstuhl and A. Sprafke, *Adv. Opt. Mater.*, 2018, **6**, 1701272.
- 20 M. Castro-Lopez, M. Gaio, S. Sellers, G. Gkantzounis, M. Florescu and R. Sapienza, *APL Photonics*, 2017, **2**, 061302.
- 21 C. De Rosa, F. Auremma, C. Diletto, R. Di Girolamo, A. Malafronte, P. Morvillo, G. Zito, G. Rusciano, G. Pesce and A. Sasso, *Phys. Chem. Chem. Phys.*, 2015, **17**, 8061–8069.
- 22 G. Zito, G. Rusciano, G. Pesce, A. Dochshanov and A. Sasso, *Nanoscale*, 2015, **7**, 8593–8606.
- 23 W. Man, M. Florescu, E. P. Williamson, Y. He, S. R. Hashemizad, B. Y. Leung, D. R. Liner, S. Torquato, P. M. Chaikin and P. J. Steinhardt, *Proc. Natl. Acad. Sci. U. S. A.*, 2013, **110**, 15886–15891.
- 24 J. Haberko, N. Muller and F. Scheffold, *Phys. Rev. A: At., Mol., Opt. Phys.*, 2013, **88**, 043822.
- 25 W. Man, M. Florescu, K. Matsuyama, P. Yadak, G. Nahal, S. Hashemizad, E. Williamson, P. Steinhardt, S. Torquato and P. Chaikin, *Opt. Express*, 2013, **21**, 19972–19981.
- 26 R. Degl'Innocenti, Y. Shah, L. Masini, A. Ronzani, A. Pitanti, Y. Ren, D. Jessop, A. Tredicucci, H. Beere and D. Ritchie, *Quantum Sensing and Nanophotonic Devices XII*, 2015, p. 93700A.
- 27 D. Chen and S. Torquato, *Acta Mater.*, 2018, **142**, 152–161.
- 28 G. Zhang, F. Stillinger and S. Torquato, *J. Chem. Phys.*, 2016, **145**, 244109.
- 29 S. Ramaswamy, *Annu. Rev. Condens. Matter Phys.*, 2010, **1**, 323–345.

- 30 I. H. Riedel, K. Kruse and J. Howard, *Science*, 2005, **309**, 300–303.
- 31 W. R. DiLuzio, L. Turner, M. Mayer, P. Garstecki, D. B. Weibel, H. C. Berg and G. M. Whitesides, *Nature*, 2005, **435**, 1271.
- 32 E. Lauga, W. R. DiLuzio, G. M. Whitesides and H. A. Stone, *Biophys. J.*, 2006, **90**, 400–412.
- 33 J. Gibbs, S. Kothari, D. Saintillan and Y.-P. Zhao, *Nano Lett.*, 2011, **11**, 2543–2550.
- 34 F. Kümmel, B. ten Hagen, R. Wittkowski, I. Buttinoni, R. Eichhorn, G. Volpe, H. Löwen and C. Bechinger, *Phys. Rev. Lett.*, 2013, **110**, 198302.
- 35 L. Caprini and U. M. B. Marconi, *Soft Matter*, 2019, **15**, 2627–2637.
- 36 M. E. Cates and J. Tailleur, *Annu. Rev. Condens. Matter Phys.*, 2015, **6**, 219–244.
- 37 I. Buttinoni, J. Bialké, F. Kümmel, H. Löwen, C. Bechinger and T. Speck, *Phys. Rev. Lett.*, 2013, **110**, 238301.
- 38 Y. Sumino, K. H. Nagai, Y. Shitaka, D. Tanaka, K. Yoshikawa, H. Chaté and K. Oiwa, *Nature*, 2012, **483**, 448.
- 39 H. Jiang, H. Ding, M. Pu and Z. Hou, *Soft Matter*, 2017, **13**, 836–841.
- 40 J. Yan, M. Han, J. Zhang, C. Xu, E. Luijten and S. Granick, *Nat. Mater.*, 2016, **15**, 1095.
- 41 E. Lushi, H. Wioland and R. E. Goldstein, *Proc. Natl. Acad. Sci. U. S. A.*, 2014, **111**, 9733–9738.
- 42 T. Sanchez, D. T. Chen, S. J. DeCamp, M. Heymann and Z. Dogic, *Nature*, 2012, **491**, 431.
- 43 A. Bricard, J.-B. Caussin, N. Desreumaux, O. Dauchot and D. Bartolo, *Nature*, 2013, **503**, 95.
- 44 M. Feng and Z. Hou, *Soft Matter*, 2017, **13**, 4464–4481.
- 45 M. Feng and Z. Hou, *Chin. J. Chem. Phys.*, 2018, **31**(4), 584–594.
- 46 A. Kaiser, H. Wensink and H. Löwen, *Phys. Rev. Lett.*, 2012, **108**, 268307.
- 47 O. Sipos, K. Nagy, R. Di Leonardo and P. Galajda, *Phys. Rev. Lett.*, 2015, **114**, 258104.
- 48 O. Chepizhko and F. Peruani, *Phys. Rev. Lett.*, 2013, **111**, 160604.
- 49 G. Volpe, I. Buttinoni, D. Vogt, H.-J. Kümmerer and C. Bechinger, *Soft Matter*, 2011, **7**, 8810–8815.
- 50 M. Mijalkov and G. Volpe, *Soft Matter*, 2013, **9**, 6376–6381.
- 51 C. Reichhardt and C. O. Reichhardt, *Phys. Rev. E: Stat., Nonlinear, Soft Matter Phys.*, 2013, **88**, 042306.
- 52 B.-q. Ai, Y.-f. He and W.-r. Zhong, *Soft Matter*, 2015, **11**, 3852–3859.
- 53 Q. Chen and B.-Q. Ai, *J. Chem. Phys.*, 2015, **143**, 09B612_1.
- 54 H. C. Fu, T. R. Powers and R. Stocker, *et al.*, *Phys. Rev. Lett.*, 2009, **102**, 158103.
- 55 A. Nourhani, Y.-M. Byun, P. E. Lammert, A. Borhan and V. H. Crespi, *Phys. Rev. E: Stat., Nonlinear, Soft Matter Phys.*, 2013, **88**, 062317.